Research article

Evolution of the sources of TTG and associated rocks during the Archean from in-situ ^{87}Sr/^{86}Sr isotope analysis of apatite by LA-MC-ICPMS

Summer A. Caton [a], Matthijs A. Smit [a,*], Robert B. Emo [a,b], Kira A. Musiyachenko [a],
Melanie Kielman-Schmitt [c], Ellen Kooijman [c], Anders Scherstén [d], Jaana Halla [e],
Wouter Bleeker [f], J. Elis Hoffmann [g], Om Prakash Pandey [h,i], Arathy Ravindran [h,j],
Alessandro Maltese [h,k], Klaus Mezger [h]

[a] Department of Earth, Ocean and Atmospheric Sciences, University of British Columbia, 2020-2207 Main Mall, Vancouver, British Columbia V6T 1Z4, Canada
[b] School of Earth and Atmospheric Sciences, Queensland University of Technology, 2 George Street, Brisbane, QLD 4000, Australia
[c] Department of Geosciences, Swedish Museum of Natural History, Frescativägen 40, SE-104 05 Stockholm, Sweden
[d] Department of Geology, Lund University, Sölvegatan 12, SE-223 62 Lund, Sweden
[e] Geological Museum, Finnish Museum of Natural History, Pohjoinen Rautatiekatu 13, FIN-00100 Helsinki, Finland
[f] Geological Survey of Canada, 601 Booth Street, Ottawa, Ontario K1A 0E8, Canada
[g] Institut für Geologische Wissenschaften, Freie Universität Berlin, Malteserstraße 74-100, D-12249 Berlin, Germany
[h] Institut für Geologie, Universität Bern, Baltzerstrasse 1+3, CH-3012 Bern, Switzerland
[i] Department of Earth Sciences and Engineering, King Abdullah University of Science and Technology (KAUST), Thuwal 23955, Saudi Arabia
[j] Institut für Geochemie und Petrologie, Eidgenössische Technische Hochschule, Clausiusstrasse 25, CH-8092 Zürich, Switzerland
[k] Institut de Physique du Globe de Paris, 1 rue Jussieu, F-75238 Paris, Cedex 05, France

ARTICLE INFO

ABSTRACT

Radiogenic isotopes provide an important means towards elucidating Archean crustal evolution. The global Hf and Nd isotope record of Archean crustal fragments has been instrumental to unveiling the history of ancient crustal growth and differentiation. The Rb-Sr system could provide valuable complementary constraints in this regard, as this system is particularly sensitive to magmatic fractionation processes, and the chemical and isotopic evolution of magma sources. Application of this system has so far been complicated, however, by its susceptibility to isotope re-equilibration or alteration of the Rb/Sr parent-daughter ratio. In-situ Sr isotope analysis of primary igneous minerals with very low Rb/Sr, such as apatite, provides a new means to determine the initial ^{87}Sr/^{86}Sr (^{87}Sr/^{86}Sr$_i$) values for igneous rocks directly. In this study, we apply in-situ Sr isotope analysis of apatite by LA-MC-ICPMS to tonalite-trondhjemite-granodiorite (TTG) rocks and end-member sanukitoids from Archean cratons worldwide. The ^{87}Sr/^{86}Sr$_i$ values of sanukitoids are relatively radiogenic, supporting the model in which such rocks are formed by flux melting of a mantle strongly enriched by metasomatism, possibly by slab-derived fluids. The ^{87}Sr/^{86}Sr$_i$ values for TTGs formed between 3.72 and 3.45 Ga are generally radiogenic, indicating aged amphibolite sources. The ^{87}Sr/^{86}Sr$_i$ values of younger TTGs are systematically lower and were derived from mafic sources that had an average age of $\leq$0.2 Gyr. This evolution matches with observations from Hf isotopes for TTGs of similar age and indicates a systematic change in the nature or efficiency of TTG crust formation during the Paleoarchean. In-situ Sr isotope analysis of apatite provides a useful method to uncover the Sr record of the early continental crust, and enables constraints on local source evolution and the general two-step evolutionary process of Archean crust formation.

1. Introduction

From its initial formation in the Archean (4.0–2.5 Ga) until the present day, the continental crust and the complementary depleted mantle reservoir have undergone major secular changes in their composition and tectonic style. The early composition of continental crust, its petrogenesis and the composition of its source are among the most enigmatic aspects to this long-term evolution (Kamber, 2015;

Moyen and Martin, 2012). The composition of the exposed plutonic Archean continental crust has become relatively well-constrained; it dominantly comprises igneous rocks or their derivates: (1) tonalite-trondhjemite-granodiorite (TTG) intrusive rocks, including their deformed and metamorphosed equivalents, which have long been interpreted as products of low-degree melting of a basaltic source in the garnet stability field (Foley et al., 2002; Hoffmann et al., 2011; Moyen and Martin, 2012; Rapp and Watson, 1995); (2) sanukitoids, which are high-Mg quartz-monzodiorites and granodiorites, characterized by high concentrations of Ni, Cr and large-ion lithophile elements (e.g., Sr, Ba), as well as strong light REE (LREE) enrichment (e.g., Halla, 2005); and (3) crust-derived or hybrid granitoids, leucogranites, and monzogranites (Laurent et al., 2014; Martin et al., 2005). Additionally, volcano-sedimentary rocks and greenstone belt lithologies make up a lesser portion of Archean crust and encompass subaqueously-erupted basalts, locally abundant komatiites, other volcanic and volcaniclastic units (the extrusive complements of the TTG suite, etc.), and sedimentary rocks. TTGs, sanukitoids, and other igneous rocks are intercalated with, or partially or totally enclose, these supracrustal sequences (Smithies, 2000).

The origins of different lithologies that constitute Archean cratons are variably ascribed to the tectonic processes that are postulated to have occurred during the Archean, which include: 1) a deformable stagnant-lid regime, with intracrustal melting and differentiation of thick, plateau-like mafic crust; 2) a sluggish-lid regime, with a deformable lithosphere and relatively localized, ephemeral proto-subduction zones; and 3) a mobile-lid regime, with some primitive form of horizontal plate tectonics and/or convective overturn, with or without associated subduction processes (Bédard, 2020; Debaille et al., 2013; Gerya, 2014; Kamber, 2015). Links between lithology, processes and tectonic setting are tenuous, with the interpretation of TTGs as a prime example. These rocks can be produced in any tectonic setting that allows melting of hydrated mafic crust at pressures high enough to stabilize garnet ± amphibole and sequester HREE (Moyen and Martin, 2012); they thus may represent ancient analogs of adakitic melts extracted from subducted mafic rocks (Foley et al., 2002; Laurent et al., 2014; Rapp et al., 2003; Smithies, 2000), or partial melts derived from tectonically or magmatically thickened mafic crust (e.g., Johnson et al., 2017; Kamber, 2015; Moyen and Martin, 2012; Nagel et al., 2012). Testing and refining such petrogenetic models require constraints on the composition and age of the sources of Archean TTGs and related rocks. Such constraints may ultimately reveal the history of crust formation and recycling going back to the first crust ever produced. Radiogenic isotope analysis provides a unique opportunity to investigate all of these aspects, which is why it has become an integral part of the global effort to unveil long-term crustal evolution and crust-mantle differentiation (e.g., Amelin et al., 1999).

Hafnium and Nd isotope analysis provides a prime means of investigating Archean crustal evolution (e.g., Vervoort and Blinchert-Toft, 1999), and has yielded invaluable constraints on crustal growth, the start of incompatible element depletion of the upper mantle, and crustal recycling (e.g., Belousova et al., 2010; Bennett et al., 1993; Dhuime et al., 2012; Hawkesworth et al., 2010; Næraa et al., 2012; Vervoort and Blinchert-Toft, 1999). The Rb-Sr system can provide a complementary and equally useful isotope tracer as the system is more sensitive to magmatic differentiation processes than Lu-Hf and Sm-Nd, owing to a stronger fractionation of Rb/Sr during magmatic differentiation (e.g., Dhuime et al., 2012). The system has been used to investigate Archean crust formation for a long time (Armstrong, 1968; Hurley et al., 1962; Moorbath and Pankhurst, 1976). However, estimating the initial $^{87}Sr/^{86}Sr$ isotope compositions ($^{87}Sr/^{86}Sr_i$) of rocks or minerals has generally been complicated by the susceptibility of the Rb-Sr system to re-equilibration. In-situ analysis of apatite — a ubiquitous accessory mineral in igneous rocks, characterized by high Sr concentrations and low Rb/Sr — can provide a means to circumvent this issue. Igneous apatite captures the initial Sr isotope composition of the earliest melts

and so provides a means to look beyond the effects of crustal assimilation and melt replenishment that occurs during later stages of magmatism (Bizzarro et al., 2003). The solubility of apatite in melts generally increases with increasing temperature, and decreasing Si concentration and degree of polymerization (London et al., 1999). For melts of tonalitic composition at the common TTG melting temperature (800–950 °C; Palin et al., 2016), apatite is not stable until the melt has cooled significant and had crystallized to at least 30% (Piccoli and Candela, 2002). Xenocrystic apatite with inherited Sr signatures thus cannot persist among TTG magmas unless perhaps fully enclosed in another xenocrystic phase. The Sr isotope signature of pristine igneous apatite in the matrix of TTGs, or included in primary igneous phases such as amphibole or plagioclase, thus represent the Sr isotope signature of the melt. This adds to the potential of Sr in apatite to constrain $^{87}Sr/^{86}Sr_i$ of TTGs.

New analytical approaches in laser ablation multi-collector inductively coupled plasma mass spectrometry (LA-MC-ICPMS; Emo et al., 2018) and secondary ionization mass spectrometry (SIMS; Gillespie et al., 2021) allow in-situ Rb-Sr isotope analysis of apatite grains at high precision and accuracy. In-situ analysis has the advantage of allowing texturally controlled investigations of apatite sequestered as inclusions in magmatic minerals, or as part of a primary igneous mineral assemblage. This approach limits the degree to which measured $^{87}Sr/^{86}Sr$ are affected by alteration and other processes that may have modified the Sr isotope signatures following primary crystallization (Emo et al., 2018; Ravindran et al., 2020). Not all inclusions are pristine and some may still have interacted with fluids if the inclusion was breached by microfractures. Such alteration can typically be identified by the elevated Rb/Sr values (Glodny and Grauert, 2009). Alteration of apatite typically leads to $^{87}Sr/^{86}Sr$ values that are higher than $^{87}Sr/^{86}Sr_i$ due to interaction of the fluids with high-Rb/Sr matrix phases. Thus, $^{87}Sr/^{86}Sr_i$ of the host rock at the time of apatite formation is typically constrained on the basis of the least-radiogenic $^{87}Sr/^{86}Sr$ values obtained from texturally primary apatite with low Rb/Sr (Emo et al., 2018; Ravindran et al., 2020).

Using $^{87}Sr/^{86}Sr_i$ determined on primary apatite to investigate source Sr-isotope signatures of (meta-)igneous rocks requires age constraints on the formation of the primary apatite-bearing assemblage. This can be done via U-Pb age constraints from either the apatite itself, or from igneous zircon in the same rock. The former would seem preferable, as it would provide both Sr and age data from the same phase. However, the U-Pb and Sr isotope systems in apatite would need to be coupled and representative of igneous crystallization. However, in contrast to Sr, Pb is relatively mobile in apatite, implying that in overprinted rocks, the U-Pb ages obtained from apatite are significantly decoupled from the still-primary Sr isotope signatures (Watson et al., 1985). This issue is particularly relevant for Archean (meta-)igneous rocks, such as TTGs, which are typically tectonically reworked and thermally overprinted. An alternative approach to obtain the required age constraints is to use the U-Pb age of igneous zircon. This study integrates the latter with in-situ Rb-Sr analysis of TTGs, sanukitoids, and related rocks from Archean cratons of various cratonic lineage and age (3.8–2.7 Ga) to investigate the evolution of sources of TTGs and related rocks throughout the Archean.

2. Geological background

Archean granitoid rocks from eight cratonic terranes of different (paleo-)geographical location and age were chosen (Fig. 1): The Southern Abitibi Greenstone Belt of the Superior Craton, Canada; the Western Karelia Subprovince (eastern and western segments) of the Karelian Craton, Finland; the Kvanefjord Block of the North Atlantic Craton, southwest Greenland; the Tasiusarsuaq Terrane of the North Atlantic Craton, southwest Greenland; the Singhbhum Craton, eastern India; the Bastar Craton of central India; and the Ancient Gneiss Complex of Eswatini and the Stolzburg Domain of the Barberton Granitoid-Greenstone Terrane of the Kaapvaal Craton, South Africa. The samples
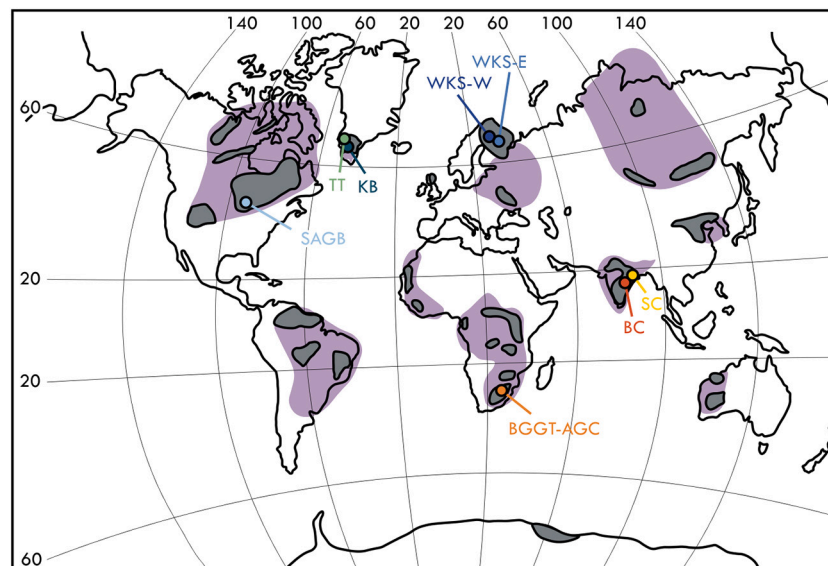
Fig. 1. Global distribution of exposed Archean continental crust (grey areas). The areas in purple are underlain by Archean-Proterozoic terranes. The field locations are denoted by the colour dot markers. The sample locations with associated lithologies and number of samples (n) are included. Map modified after Bleeker (2003). (For interpretation of the references to colour in this figure legend, the reader is referred to the web version of this article.)

were chosen from large suites of samples for their relatively pristine mineral assemblages and low abundance of secondary minerals.

2.1. Southern Abitibi Greenstone Belt

The Southern Abitibi Greenstone Belt (SAGB) represents a crustal segment of the Superior Craton in Canada. Diverse volcanic assemblages of komatiite, tholeiite, and calc-alkaline mafic to felsic lavas erupted between 2750 and 2688 Ma (Ayer et al., 2002). The intercalation of these assemblages with plutonic intrusions may suggest a complex interaction between the varying magma sources of these different rocks within a changing geodynamic environment (Ayer et al., 2002). There are three suites of plutonic rocks comprising the SAGB: (1) *syn*-volcanic intrusions (c. 2750 to 2688 Ma) of similar composition to the volcanic assemblages; (2) syn-tectonic tonalite-granodiorite intrusions (2690–2680 Ma); and (3) c. 2665 to 2640 Ma intrusions consisting of biotite granite, pegmatite, and S-type granite. Peak metamorphism occurred from 2677 to 2643 Ma, with grades ranging from (sub) greenschist to amphibolite facies (Corfu, 1993; Ayer et al., 2002). Three granitoid samples were investigated from a foliated tonalite suite (sample *BNB-14-027*), a diorite-monzodiorite-granodiorite suite (sample *BNB-14-029*), and a massive granodiorite-granite suite (sample *BNB-17-080b*).

Sample *BNB-14-027* is a foliated tonalite consisting mostly of plagioclase and quartz, with minor orthoclase and hornblende, and biotite, titanite, apatite, zircon, and accessory Fe-oxides. Sample *BNB-14-029* is a quartz monzodiorite consisting of plagioclase, quartz, orthoclase, and hornblende, and accessory biotite, titanite, clinopyroxene, apatite, zircon, and Fe-oxides. Sample *BNB-17-0808b* is a highly sericitized monzodiorite mainly consisting of plagioclase with minor quartz, hornblende and orthoclase and clinopyroxene, biotite, titanite, apatite, zircon and accessory Fe-oxides. The presence of secondary phases such as epidote, muscovite, chlorite, and sericite in all three of these samples suggests metamorphism between greenschist and lower amphibolite-facies conditions.

2.2. Karelia Province

The Archean cratonic nucleus of the Fennoscandian (Baltic) Shield is divided into the Norrbotten, Murmansk, Kola, Belomorian, and Karelia

Provinces. The Karelian Province, located in eastern Finland and western Russia, preserves 3.5 to 2.6 Ga rocks and is subdivided into three subprovinces: the Western Karelia Subprovince (WKS), Central Karelia, and the Vodlozero Subprovince (Hölttä et al., 2012). The Karelian Province is largely comprised of gneissic granitoids, classified into four main groups: TTGs (3.50–2.73 Ga), sanukitoid granitoids (2.74–2.72 Ga), quartz diorite-quartz monzodiorites (c. 2.70 Ga), and granodiorite-granite-monzogranites (2.71–2.66 Ga). Additionally, the TTG complexes, with migmatitic amphibolite layers and inclusions, were metamorphosed at amphibolite to granulite-facies conditions at 2.70–2.60 Ga (Hölttä et al., 2012). Greenstone belt assemblages representing a variety of geodynamic settings are also present in the Karelian Province (Hölttä et al., 2012). This study encompasses rocks from the WKS. The subprovince is further divided into eight complexes (Hölttä et al., 2012). Samples were collected from the Lentua complex in the eastern terrane (WKS-E), and the Siurua and Ranua complexes in the western terrane (WKS-W).

2.2.1. Western Karelia Subprovince, eastern segment

The eastern segment of the WKS-E comprises mainly Neoarchean (<2.8 Ga) plutonic and volcanic rocks, with relatively abundant sanukitoid granitoids and greenstone belts (Hölttä et al., 2012). The Lentua Complex in the eastern part of the WKS-E includes 2.95–2.73 Ga TTGs and the c. 2.72 Ga sanukitoid series intrusions that are c. 20 Ma younger than sanukitoids in the Ilomantsi Complex of the adjacent Central Karelia Subprovince. The samples for this study were collected from porphyritic Koitere granodiorites (2722 ± 6 Ga; Heilimo et al., 2011) of uniform sanukitoid-type geochemical characteristics (Halla, 2005). These rocks are divided into two groups: undeformed high-grade pyroxene-bearing granodiorites (Group L1) and variably deformed gneisses (Group L2). The metamorphosed granodiorites of Group L1 contain orthoclase, plagioclase, quartz, clinopyroxene locally associated with orthopyroxene or hornblende, and biotite, as well as accessory apatite, titanite, zircon, and Fe-oxides. Secondary minerals include sericite, epidote, chlorite, and muscovite. Group L2 contains variably deformed granitoids that contain porphyritic orthoclase and plagioclase. The matrix consists of quartz, feldspars, biotite, epidote and chlorite, and accessory apatite, zircon, titanite, and Fe-oxides. The secondary minerals include sericite, epidote, chlorite, and muscovite (Halla, 2002). Six samples were collected from the Koitere granodiorites, three from

Group L1 (samples *PK-27*, *PK-45*, and *PK-50*), and the others representing Group L2. The samples are variably deformed, from pristine (*PK-50* and *PK-45*) to protomylonitic (*PK-42*, *PK-27*, *PK-100*) and mylonitic (*PK-47*; Halla, 2005). Of these, only sample *PK-100* exhibits significant secondary epidote, muscovite, sericite, and chlorite. A zircon $^{207}Pb/^{206}Pb$ age of 2722 ± 6 Ma was previously obtained for sample *PK-50* and interpreted to represent sanukitoid emplacement in the WKS-E (Heilimo et al., 2011); this age is used as the age constraint for all samples from this subprovince.

2.2.2. Western Karelia Subprovince, western segment

The western segment of the Western Karelia Subprovince (WKS-W) mostly comprises migmatitic TTG orthogneisses and amphibolites metamorphosed to medium- to low-pressure granulite facies conditions. Sanukitoids are less common in the WKS-W compared to the WKS-E. The Siurua trondhjemite gneisses retain the oldest age components recognized within the Fennoscandian Shield (Mutanen and Huhma, 2003). These rocks occur in association with granulite-facies orthopyroxene-bearing TTG orthogneisses and amphibolites (c. 2.96 Ga). The Ranua complex consists of 2.82–2.73 Ga TTGs and 2.70–2.62 Ga granites (Hölttä et al., 2012). The 2.70 Ga Ranua intrusion in the north ranges in composition from diorite to quartz diorite (Hölttä et al., 2012).

Two samples were selected for this study: one from the Siurua trondhjemite gneisses (sample *EK-2-1E*) and one sample from the Ranua complex (sample *EK-1-1*). Sample *EK-1-1* is a quartz diorite consisting of plagioclase and quartz with minor amphibole, biotite, apatite, zircon and Fe-oxides. Sample *EK-2-1E* is a trondhjemite gneiss consisting of quartz and plagioclase with accessory biotite, apatite, zircon and Fe-oxides. Although the samples were the most pristine among the samples from these complexes, the local presence of chlorite, muscovite, and sericite suggests metamorphism at greenschist conditions.

2.3. Kvanefjord Block

The Kvanefjord Block (KB) is one of six shear-zone bounded crustal blocks of the North Atlantic Craton in southern West Greenland. The KB represents a 130 km-long Mesoarchean crustal segment subdivided into the Paamiut block, and the overlying allochthonous Neria nappe. The KB generally comprises amphibolite- to granulite-facies orthogneisses (Windley and Garde, 2009). Initial studies suggested the block consists of individual tectonothermal terranes with different metamorphic histories separated by tectonic boundaries that had developed following granulite-facies metamorphism (Friend and Nutman, 2001). However, it has also been interpreted as a contiguous crustal segment with a transition from upper amphibolite facies in the south to lower granulite facies in the north. Mesoarchean tonalite gneiss samples were investigated from the Kvanefjord-Neria Nappe (*518001*) and the Tartôq Greenstone Belt (*508281*). Sample *518001* is a foliated tonalite that dominantly contains quartz, plagioclase and biotite, with accessory zircon and apatite. Sample *508281* is a weakly foliated tonalite consisting mainly of quartz, plagioclase and biotite with minor K-feldspar and epidote, as well as accessory zircon and apatite. The presence of secondary epidote indicates metamorphic overprint at upper greenschist- to lower amphibolite-facies conditions. Zircon U-Pb ages determined by LA-ICPMS yielded ages of 2875 ± 20 Ma (sample *508,281*) and 2835 ± 15 (sample *518,001*; Smit et al., 2019).

2.4. Tasiusarsuaq Terrane

The Neoarchean Tasiusarsuaq Terrane (TT) is a 400 km-wide crustal segment situated in the North Atlantic Craton in southern West Greenland. The TT comprises predominantly TTG gneisses that were emplaced at 2.92 to 2.82 Ga, and additionally includes Archean supracrustal rocks, which were metamorphosed at granulite-facies conditions. The TTGs were intruded by granite dykes (2.83–2.80 Ga) and tonalite dykes (c. 2.77 Ga; Kolb et al., 2012). Peak granulite-facies metamorphism occurred at c. 2.80 Ga, possibly due to crustal thickening (Kolb et al., 2012). Apatite from three samples from the TT was analyzed (*508276*, *518018*, and *518022*). Sample *508,726* is a granodiorite consisting mostly of plagioclase, quartz, biotite and minor K-feldspar, and includes the accessory apatite, zircon, titanite, and Fe-oxides. Sample *518018* is a granodiorite consisting of plagioclase, quartz, hornblende, K-feldspar and biotite, and includes accessory apatite, zircon, titanite, and Fe-oxides. This sample does not contain any secondary phases. Sample *518022* is a tonalite that contains primarily plagioclase, quartz, K-feldspar, hornblende and biotite with minor pyroxene and accessory apatite, titanite, zircon, and Fe-oxides. The samples were metamorphosed at greenschist to granulite facies conditions.

2.5. Singhbhum Craton

The Singhbhum Craton (SC) is one of four major Archean cratons of the Indian Shield, which includes the Bastar, Dharwar, and Aravalli-Bundelkhand cratons. The SC, covering approximately 40,000 km², is exposed in eastern India and is underlain by Paleoarchean TTGs and potassic granites that are surrounded by greenstone belts (Pandey et al., 2019). It is comprised of three dominant components: (1) metasedimentary and igneous rocks (greenschist- to amphibolite-facies); (2) TTGs; and (3) granitoids and tonalites of the Singhbhum Granite, which formed by partial melting of mafic crust between 3.5 and 3.3 Ga (Pandey et al., 2019; Upadhyay et al., 2014). Two samples were selected for this study (samples *Om 9c* and *Om10b*).

Sample *Om 9c* is a trondhjemite consisting mainly of quartz, plagioclase and biotite, with apatite, titanite, zircon and Fe-oxides. Sample *Om 10b* is a clinopyroxene-bearing diorite consisting of quartz, plagioclase, clinopyroxene, minor hornblende and K-feldspar, and includes accessory apatite, zircon and titanite. The presence of epidote, muscovite, chlorite (*Om 10b*), and sericite indicates these rocks were metamorphosed at greenschist to amphibolite facies conditions. Whole rock major-trace element geochemistry, Sr-Nd whole-rock isotope data, and in situ zircon U-Pb ages (3.47–3.28 Ga) and Hf isotope data for these samples have been documented previously (Pandey et al., 2019; Upadhyay et al., 2014). The samples are from magmatic bodies that formed at c. 3.35 (*Om 9c*), and 3.44 Ga (*Om 10b*; Pandey et al., 2019).

2.6. Bastar Craton

The Bastar (or Bhandara) Craton (BC) of central India covers an area of ~200,000 km² (Ghosh, 2004). The BC is bounded by two major mobile belts (the Eastern Ghats Mobile Belt to the SE and the Central Indian Tectonic Zone to the NW), and two upper Paleozoic-Mesozoic rifts, the Mahanadi graben to the NE and the Pranhita-Godavari rift to the SW (Rajesh et al., 2009). The crustal block contains 2.60–2.50 Ga TTG gneisses and greenstone belts with enclaves of 3.65–3.50 Ma tonalite gneiss (Maltese et al., 2021). The BC largely consists of: variably deformed TTG gneisses; associated supracrustal greenstone belts consisting of metamorphosed sedimentary and magmatic rocks; and distinct NW-SE trending dominantly sub-alkaline tholeiitic basaltic dyke swarms and some boninite dykes (Rajesh et al., 2009). Final stabilization of the craton occurred with the emplacement of Neoarchean-Paleoproterozoic granitoids.

Two TTG samples from the Bastar Craton were selected for this study (samples *AMA-01* and *AMA-04*). Both samples represent Paleoarchean tonalite gneiss, containing plagioclase, K-feldspar, quartz, and biotite with zircon and apatite present as accessory minerals. Muscovite is present as a secondary phase. Previous U-Pb dating using LA-ICPMS (Maltese et al., 2021) yielded the ages of 3543 ± 18 Ma (sample *AMA-04*) and 3501 ± 8 Ma (sample *AMA-01*), constraining the crystallization of the protolith of these samples.

2.7. Kaapvaal Craton

The Barberton granitoid-greenstone terrane (BGGT) of the Eastern Kaapvaal Craton in South Africa formed between 3.51 and 3.11 Ga (Moyen et al., 2007) and hosts the Barberton Greenstone Belt comprising purported ocean-floor sequences and oceanic-arc composite rocks that amalgamated with the Ancient Gneiss Complex (AGC) at c. 3.2 to 2.1 Ga (Agangi et al., 2018). Rocks older than 3.42 Ga in the BGGT proper are represented by the high-grade "Stolzburg Domain" (Moyen et al., 2007). Samples in this study are from the AGC and from the Stolzburg Domain.

2.7.1. Barberton Granitoid-Greenstone Terrane

Following the formation of the Barberton greenstone belt, extensive granitoid magmatism occurred with the emplacement of diapiric TTG plutons (c. 3.45 Ga), contributing to the thickening and stabilization of the craton. The Stolzburg Domain granite terrane represents the oldest rocks surrounding the Barberton greenstone belt and contains the Stolzburg and Theespruit plutons. These TTG plutons were emplaced between 3.46 and 3.44 Ga and intruded into the lowermost formations (Onverwacht Group, 3.55–3.30 Ga) of the greenstone belt. The Stolzburg and Theespruit plutons are predominately comprised of undeformed leucocratic trondhjemites (Anhaeusser, 2010). Three samples were investigated from the Stolzburg Domain (samples *BA-127A, BA-131* and *BA-187*).

Sample *BA-127A* is a trondhjemite from the Stolzburg pluton comprised mainly of plagioclase, quartz, K-feldspar and biotite, with accessory apatite, titanite, zircon and Fe-oxides. Sample *BA-131* is an undeformed trondhjemite from the Theespruit pluton containing primarily plagioclase, quartz, biotite, and K-feldspar, with minor pyroxene and amphibole, and apatite, titanite, zircon and Fe-oxides. Sample *BA-187* is also a trondhjemite from the Theespruit pluton comprised of plagioclase, quartz, K-feldspar and biotite, with minor orthopyroxene and amphibole, as well as accessory apatite, titanite, zircon and Fe-oxides. Secondary epidote, muscovite, chlorite, and sericite indicate these samples were metamorphosed at amphibolite-facies conditions. Zircon from samples *BA 127A* and *BA 131* yielded ^{207}Pb/^{206}Pb ages of 3457 ± 2 Ma and 3440 ± 5 Ma (Kröner, unpublished data; Kamo and Davis, 1994).

2.7.2. Ancient Gneiss Complex

The AGC comprises granitoid gneisses that range in age from 3.66 to 3.20 Ga. The Ngwane Gneiss, the oldest in the complex (3.66–3.45 Ga), includes dominantly grey gneisses interlayered with amphibolites and is locally deformed and migmatized. Younger plutonic rocks intruded older (>3.45 Ga) components between 3.45 and 3.20 Ga. Of these, the Tsawela Gneiss (3.48–3.43 Ga) occurs as intrusions into parts of the Ngwane Gneiss and is comprised of foliated diorite to tonalite gneisses, and locally records amphibolite- to granulite-facies overprinting (Hoffmann et al., 2016). Three AGC samples were investigated; two are from the Ngwane gneisses (samples *AGC-206* and *AGC-507*) and one from the Tsawela gneisses (sample *AGC-491*).

Sample *AGC-206* is a trondhjemite gneiss containing mostly quartz, plagioclase, biotite, and minor K-feldspar, including apatite, zircon and titanite as accessory minerals. Sample *AGC-507* is a grey trondhjemite gneiss comprised mainly of quartz, plagioclase, biotite and hornblende, with minor K-feldspar, and accessory apatite and zircon. Sample *AGC-491* is a tonalite gneiss largely containing plagioclase, quartz, hornblende, biotite with minor K-feldspar, as well as accessory apatite, titanite, and zircon. The presence of secondary minerals such as epidote, muscovite, chlorite, and sericite suggest the rocks of the AGC were metamorphosed to amphibolite conditions. Previous U-Pb SHRIMP dating of zircon from samples *AGC-206* and *AGC-507* yielded ^{207}Pb/^{206}Pb ages of 3620 ± 2 Ma (same as *AGC207*; Kröner et al., 2014) and 3568 ± 1 Ma (Kröner and Hoffmann, 2016), respectively.

3. Analytical methods

The methods pertaining to accessory mineral imaging, whole-rock trace-element analysis and zircon U-Pb geochronology are provided in Supplementary Text S1. Whole-rock trace-element data are provided in Figs. 2 and 3, and Supplementary Table S1. Zircon U-Pb data is provided in Fig. S1, and Supplementary Tables S2 and S3. The methods for apatite analysis are provided below.

3.1. Apatite textural classification

Apatite grains were divided into three textural categories (Figs. 4, 1) inclusions (partial or complete) in primary magmatic minerals such as amphibole or plagioclase; (2) grains embedded between primary plagioclase, amphibole, or quartz; and (3) grains that occur in more complex matrix settings, e.g., on triple or quadruple junctions between primary minerals, or in micro-domains that contain secondary phases (e. g., biotite, muscovite, epidote). The grains were imaged using high-contrast backscatter electron (BSE) imaging. Although inherited cores are extremely unlikely to persist in TTG melts, the grains were screened carefully to ensure the absence of such material. Inherited cores, as commonly seen in apatite from melts that are much more siliceous and have a lower melting temperature than TTGs, would be clearly visible in BSE images (Tepper and Kuehner, 1999). Such imaging provides a useful means of detecting polyphase apatite grains, especially in cases where the compositional zoning for common trace elements (e.g., REE) have become diffusively relaxed (Tepper and Kuehner, 1999). Consistent with expectations, no such cores were observed in the apatite grains analyzed in this study. All analyzed grains are monophase.

3.2. Apatite laser ablation micro-sampling

The Rb-Sr isotope compositions of apatite grains were determined by LA multi-collector (MC) ICPMS using a Nu Instruments *Plasma II* MC-ICPMS connected to an ESI *NWR193UC* LA system at the Vegacenter, following the analytical method developed by Emo et al. (2018). A spot size of 70 μm was used to achieve acceptable precision. All apatite grains with a cross sectional area in thin section large enough to fit such a spot were analyzed. Grains with smaller cross sectional area were not analyzed. Apatite grains identified in the analyzed samples are typically larger than 70 μm; grains with smaller cross sectional area are not actually smaller grains and thus no bias is introduced by the analytical procedure. Due to the high thermal expansion coefficient of apatite, in-situ LA micro-sampling of apatite in thin section is complicated by the high risk of grains becoming dislodged or excited from the ablation site during analysis. This risk is particularly high for small apatite grains, as commonly found in TTGs, which is why apatite is typically analyzed in thick sections (Bizzarro et al., 2003), or separated and analyzed as individual grains held in epoxy mounts (e.g., Ravindran et al., 2020). Apatite grains from the KB and BC TTGs, which were exclusively derived from matrices, were analyzed using the latter approach. Various experiments were done to prevent grain excitation. It was found that apatite can effectively be kept in place during ablation by covering thin sections with transparent industrial-grade sticky tape; ablation of the tape exposes apatite within a few laser shots, while leaving the surrounding tape intact. This method was applied to all other samples, enabling preservation of textural context.

3.3. Apatite Rb-Sr isotope analysis

All apatite grains were analyzed at a spot size 70 μm using a laser fluence of 2.7 J cm^{-2}, a repetition rate of 15 Hz, and an ablation time of 30 s (for samples) and 50 s (for reference materials). Multiple analyses were performed on single grains that were sufficiently large. Baseline was analyzed for 40 s to allow for precise corrections for isobaric interferences. These interferences were corrected for following the
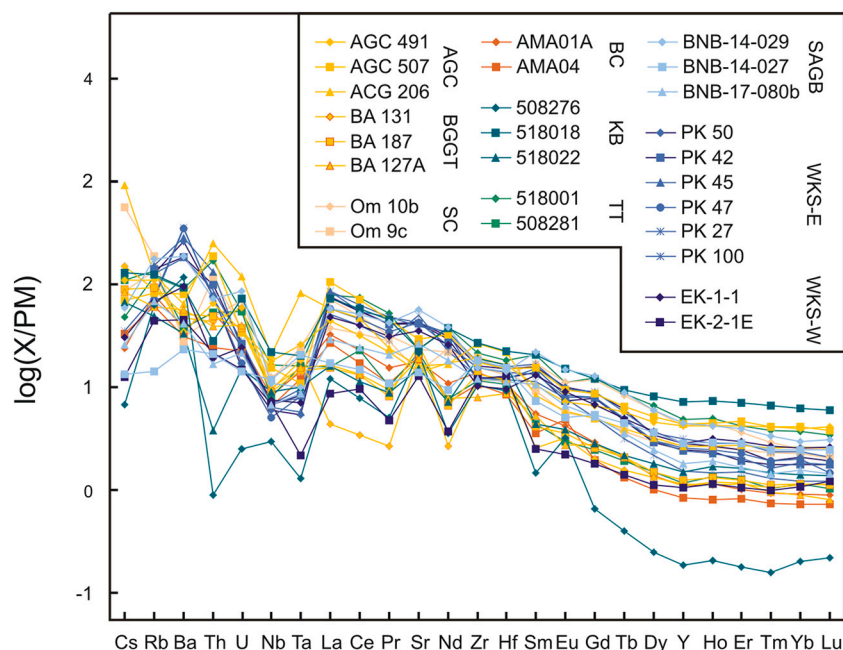
Fig. 2. Trace-element composition for the TTGs and sanukitoids subjected to Sr isotope analysis in this study. All data normalized to primitive mantle values (McDonough and Sun, 1995).
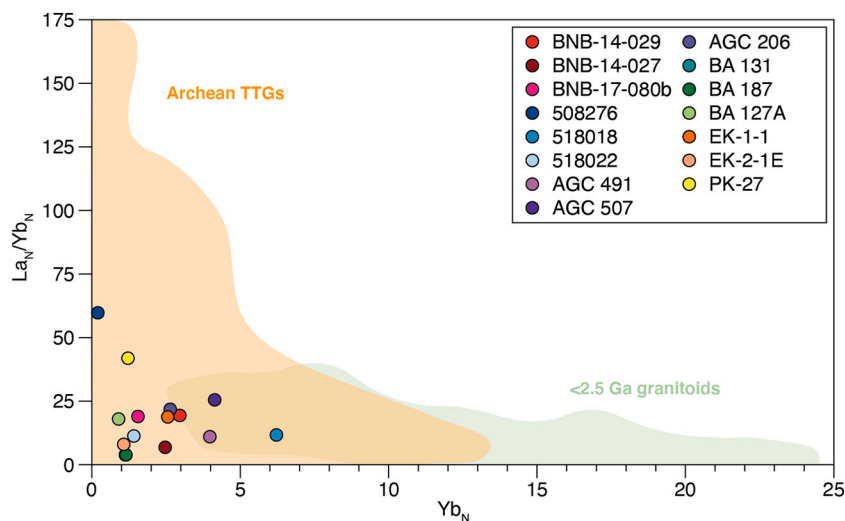

Fig. 3. Trace-element classification diagram for plutonic rocks (after Moyen and Martin, 2012). All samples show La_N/Yb_N and Yb_N values that are common among Archean TTG. Data provided as Supplementary Table S1. Subscript N marks normalization to primitive mantle values (McDonough and Sun, 1995).

analytical protocol of Emo et al. (2018). The *Durango* apatite was used as the primary reference material ($^{87}Sr/^{86}Sr = 0.706328 \pm 0.000002$; Yang et al., 2014) to monitor and correct for any drift during the course of the analysis. External reproducibility of *Durango* $^{87}Sr/^{86}Sr$ during the course of the analysis period was 48 ppm ($n = 138$). The in-house *Holly Springs* hydroxyl-apatite (*HA*), which has an $^{87}Sr/^{86}Sr = 0.718926 \pm 0.000014$ (determined via TIMS at the Vegacenter) and a different composition to *Durango* (Rb/Sr ~8 and Yb/Sr 30 times higher), was used to monitor accuracy. A weighted mean $^{87}Sr/^{86}Sr$ value of 0.71908 ± 0.00013 ($n = 16$; MSWD = 1.02; Table S4) was obtained, which indicates the inter-ference corrections are accurate and robust within the uncertainty of a typical analysis of apatite as unknown.

All measured $^{87}Sr/^{86}Sr$ values were corrected for in-situ produced radiogenic ^{87}Sr using the crystallization age and a $\lambda^{87}Rb$ of 1.393×10^{-11} yr^{-1} (Nebel et al., 2011) and are reported as such. Analyses of

unknowns with Rb/Sr values high enough that radiogenic ingrowth corrections would exceed typical analytical error were removed ($n = 8$; c. 0.05 for Archean ages), as were analyses with particularly high Yb/Sr values (> 0.006; $n = 22$), as these likely do not represent pure apatite. Analyses of apatite in the different rock samples (after data filtering) yielded a weighted mean $^{84}Sr/^{86}Sr$ value of 0.05649 ± 0.00004 ($n = 318$; MSWD = 1.6). This is indistinguishable from the recommended value of 0.05655 ± 0.00014 (Moore et al., 1982), indicating general accuracy of the corrections for mass bias and isobaric interferences from Kr^+, REE^{2+}, Ca and CaAr dimers. Data with $^{84}Sr/^{86}Sr$ values outside 2σ of the mean were omitted. The $^{87}Sr/^{86}Sr$ results are provided in Table S5 and shown in Figs. 5 and 6. To investigate whether the tape had any effect on the analyses, the Madagascar (*MAD*) apatite reference ($^{87}Sr/^{86}Sr = 0.71180 \pm 0.00011$; Yang et al., 2014) was analyzed, using an uncovered *Durango* apatite as primary reference. The analyses
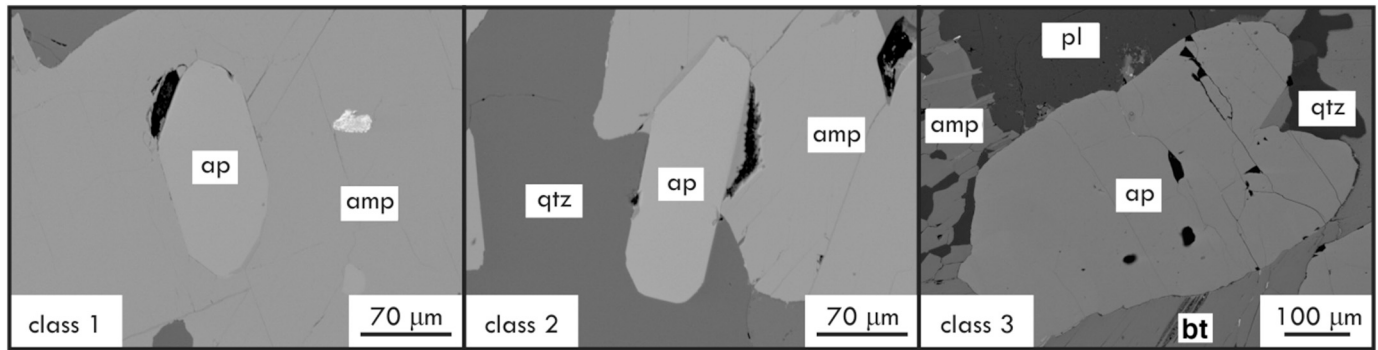
Fig. 4. Backscatter electron images showing apatite in the three textural classes 1) inclusions in primary igneous mineral grains, 2) grains embedded in such grains, and 3) matrix grains.
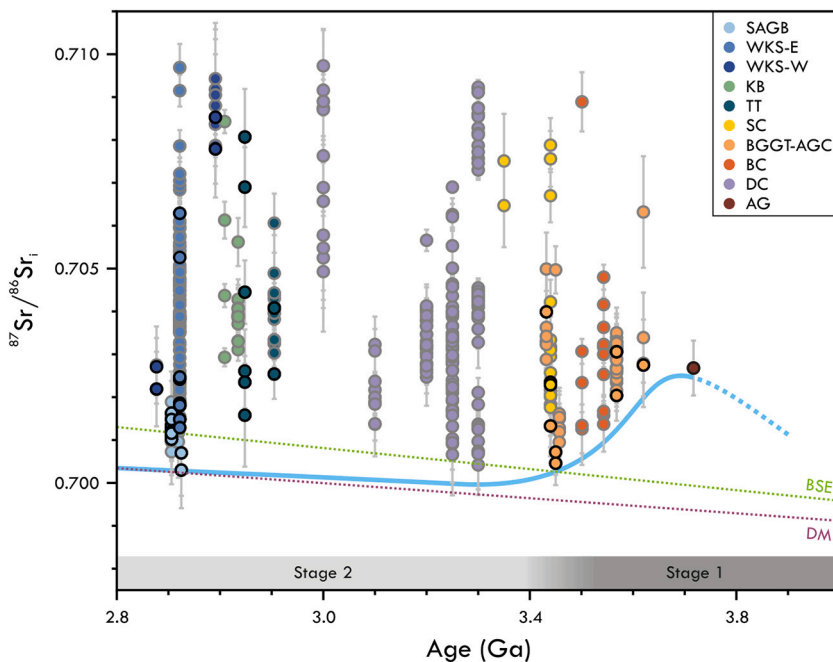

Fig. 5. Apatite initial $^{87}Sr/^{86}Sr$ vs. age for Archean TTGs measured by LA-MC-ICPMS. SAGB (Southern Abitibi Greenstone Belt); BGGT-AGC (Barberton Granitoid-Greenstone Terrane-Ancient Gneiss Complex); TT (Tasiusarsuaq Terrane, North Atlantic Craton); WKS-E (Western Karelia Subprovince-East); WKS-W (Western Karelia Subprovince-West); SC (Singhbhum Craton); KB (Kvanefjord Block), and BC (Bastar Craton). DC (Dharwar Craton; data from Ravindran et al., 2020); AG (Acasta Gneiss; datum represents weighted mean of 7 Sr isotope analyses of apatite inclusions in zircon determined by Emo et al., 2018). The blue curve follows the least radiogenic $^{87}Sr/^{86}Sr_i$ values and traces the inferred isotope evolution of Eoarchean crust, as determined for the Acasta Gneiss by Emo et al. (2018). Data from inclusions in relict magmatic minerals are shown with black outline; other data represent apatite in other or unknown textural settings. The BSE reference line and the depleted MORB mantle (DM) evolution line is as explained in the text. (For interpretation of the references to colour in this figure legend, the reader is referred to the web version of this article.)

yielded identical weighted mean $^{87}Sr/^{86}Sr$ values of 0.71167 ± 0.00014 ($n = 8$; MSWD = 0.51) and 0.71165 ± 0.00008 ($n = 23$; MSWD = 0.42) with and without tape, respectively (Supplementary Table S6). This indicates the data from apatite analyses with and without tape cover are indistinguishable and equally accurate.

4. Results

4.1. Whole-rock trace element compositions

Most of the 26 samples studied show negative Nb-Ta anomalies, generally positive Sr anomalies, and no resolvable Eu anomalies relative to primitive mantle (Fig. 2; Table S1). The analyses include rocks with highly fractionated REE patterns (La_N/Yb_N from 3.9 to 60; Fig. 3), which are indicative of either partial melts formed in the garnet-stability field of mantle peridotites, or formed from a mafic source with residual garnet. Trace element data from WKS-E samples (excluding *PK-27*), originally presented by Halla (2002) and shown here for reference, show highly fractionated REE patterns, with $(La/Yb)_N$ values ranging from 15.7 to 46.3. All five samples display negative Nb-Ta anomalies, a slightly negative Eu anomaly (Eu/Eu* range from 0.69 to 0.81). The REE patterns of the Koitere sanukitoids resemble calc-alkaline plutons with

higher HREEs than average TTGs. Similar to other sanukitoids, these samples show high LILE (Sr, Ba) and LREE concentrations (Halla, 2002). Samples from the KB show different trace-element compositions. Sample *518,001* is of the high-Yb TTG variety with primitive mantle-normalized Yb (Yb_N) of 4.0–4.8, whereas sample *508,281* is of the low-Yb TTG variety with Yb_N between 0.39 and 1.2. All KB samples exhibit a negative Nb-Ta anomaly, and elevated Zr and Hf concentrations, and plot on the low-La_N/Lu_N end of Archean TTG array. The REE distributions for the SC samples show elevated LREE, and depleted HREE to varying degrees. Samples additionally exhibit a negative Nb anomaly in the absence of Ta, elevated Pb, Sr, Zr, and Hf, and a slight Eu anomaly. The BC samples have low Yb_N values (0.77; *AMA-04* and 0.97; *AMA-01A*; Fig. 3) and elevated LREE concentration, and exhibit a negative Nb-Ta anomaly, positive Sr and Zr-Hf anomalies, and no Eu anomaly. In general, it is assumed that samples with strongly elevated HREE and higher Yb_N and lower La_N/Yb_N (e.g., *AGC-491*, *AGC-507*, and *518,018*; Fig. 3) may indicate garnet-free melting, as is commonly indicated for post-2.5 Ga granitoids (Fig. 3; Moyen and Martin, 2012). Taken together, all the samples in this study cover the range in trace-element compositions that typifies Archean TTGs (Moyen and Martin, 2012).
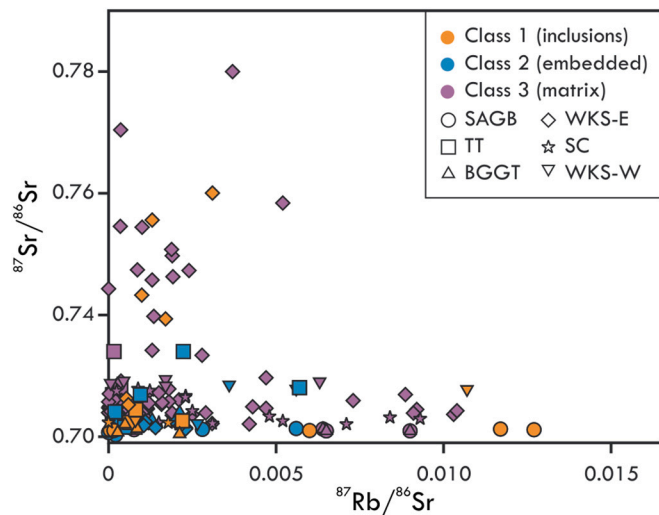
Fig. 6. $^{87}Sr/^{86}Sr$ vs. $^{87}Rb/^{86}Sr$ of all apatite classes. Plotted data includes only data post-filtering (Rb/Sr values >0.05; Yb/Sr values >0.006; $^{84}Sr/^{86}Sr$ values outside 2σ of the mean). Class 1 (inclusions), Class 2 (grains embedded in igneous phases), and Class 3 (matrix grains). Shape of symbols indicates the source location.

4.2. Apatite Sr isotope compositions

Apatite from the samples analyzed in this study show a large range in $^{87}Sr/^{86}Sr$ values (Fig. 5). Analyses within single grains are typically identical within analytical uncertainty. A broad correlation between $^{87}Sr/^{86}Sr$ values and texture is observed for most of the samples. Both inclusions in (Class 1), and grains between, primary igneous phases (Class 2), generally yielded lowest $^{87}Sr/^{86}Sr$ values (Fig. 6). They likewise show a similar range in $^{87}Rb/^{86}Sr$ values, which are largely below 0.01. Exceptions are some inclusions that yielded significantly more radiogenic $^{87}Sr/^{86}Sr$ values than matrix grains in the same sample (Fig. 5). Matrix apatite (Class 3) records larger ranges in $^{87}Sr/^{86}Sr$ values, with highly radiogenic values above 0.71. Class 3 apatite shows a higher incidence of elevated $^{87}Rb/^{86}Sr$ (>0.005) and $^{87}Sr/^{86}Sr$ values (>0.71). Elevated radiogenic $^{87}Sr/^{86}Sr$ values in Class 2 and 3 apatite are typically associated with micro-domains containing biotite and K-feldspar.

Apatite in TTGs from the AGC, BC and BGGT (3.62–3.44 Ga) yields minimum $^{87}Sr/^{86}Sr$ values between 0.7028 ± 0.0007 and 0.7005 ± 0.0005, decreasing with age. The lowest $^{87}Sr/^{86}Sr$ observed for younger TTGs are between 0.7016 ± 0.0012 and 0.7003 ± 0.0009. The latter is indistinguishable to that observed among BGGT TTGs. The lowest $^{87}Sr/^{86}Sr$ observed for the c. 2.7-Ga WKS-E sanukitoids is 0.7022 ± 0.0009. For these rocks, there is no relationship between the degree of deformation and $^{87}Sr/^{86}Sr$. In general, there is no resolvable correlation between trace-element composition or ratios (e.g., Gd/Yb, La/Sm, Ba/Nb) and age, or the range or minima of Sr isotope values of apatite for the given samples.

5. Discussion

5.1. Significance of Sr isotope signature in apatite

Continental rocks that derive partially or wholly from significantly older crustal rocks will have elevated $^{87}Sr/^{86}Sr$ values compared to the mantle that these plutonic rocks derive from (Arndt, 2013). The spread in $^{87}Sr/^{86}Sr_i$ values observed here for the apatite grains in single samples is nevertheless too extreme to be reasonably explained by differences in the degree of crustal contribution to an evolving melt. The isotope heterogeneity is likely largely the result of secondary processes. Apatite

in diorites that were subject to open-system fluid-rock interaction and Rb-Sr re-equilibration typically exhibits high Rb/Sr values (Glodny and Grauert, 2009). If such a process is responsible for the elevated $^{87}Sr/^{86}Sr_i$ values observed among embedded (Class 2) and matrix (Class 3) apatite, then a correlation would be expected between Rb/Sr and $^{87}Sr/^{86}Sr_i$ values. Such a correlation is not observed (Fig. 6), indicating that the source of the ^{87}Sr enrichment, as observed in some of the analyzed apatite grains, may instead be the local environment or assemblage that apatite grains occur in. Considering the susceptibility of isotope re-equilibration of the Rb-Sr system in minerals such as biotite (e.g., Jenkin et al., 2001), it is possible that matrix apatite incorporated radiogenic ^{87}Sr from high-K and Rb phases within the rock (Wasserburg et al., 1964; Watson et al., 1985). This would be consistent with the high incidence of radiogenic $^{87}Sr/^{86}Sr_i$ in micro-domains containing K-rich phases such as biotite or K-feldspar, indicating that the source of ^{87}Sr enrichment may be local. Whether Sr re-equilibration occurred via diffusive exchange, fluid-mediated mineral replacement or otherwise is not clear. Regardless of the exact process, it affected apatite grains in their entirety, considering that $^{87}Sr/^{86}Sr$ values for multiple spots in single grains were largely identical, independent of $^{87}Sr/^{86}Sr$ value.

Analyzing apatite inclusions sequestered in primary igneous minerals significantly limits the degree to which Sr isotope ratios may be influenced by Sr isotope re-equilibration (e.g., Emo et al., 2018). This is also illustrated by this study, where apatite inclusions in primary minerals typically yield relatively low, or even the lowest, $^{87}Sr/^{86}Sr_i$ values observed for given samples, and the incidence of radiogenic values is significantly lower than among matrix apatite grains. Exceptions to this illustrate that secondary ^{87}Sr enrichment cannot be a priori ruled out for such inclusions, even if they seem pristine and intact. Re-equilibration of these inclusions may have occurred by fluid-mediated Sr exchange through micro-cracks that were either fully healed or not in the plane of the thin section. Estimates of $^{87}Sr/^{86}Sr_i$ for re-equilibrated apatite cannot be confidently linked to the crystallization age of the rock and its primary mineral assemblage and are thus geologically meaningless. Given that re-equilibration may have been partial and $^{87}Sr/^{86}Sr$ thus may be mixed, highly radiogenic $^{87}Sr/^{86}Sr$ values for given samples are not included in the interpretation. Instead, the general approach is adopted to conservatively treat the least radiogenic measured $^{87}Sr/^{86}Sr$ values from apatite as the closest approximation of the $^{87}Sr/^{86}Sr_i$ value of the host rock at the time of crystallization from a melt, and interpret consistent minima of cogenetic samples and (sub-)terranes as geologically meaningful (e.g., Ravindran et al., 2020).

5.2. The meaning of apatite $^{87}Sr/^{86}Sr_i$ values from Archean TTGs and sanukitoids

The lowest $^{87}Sr/^{86}Sr_i$ estimates of apatite in the Archean TTGs and related granitoids analyzed in this study differ through time. In spite of the relative complexities of the overall dataset, two broad stages can be identified in the evolution of $^{87}Sr/^{86}Sr_i$ values of Archean TTGs relative to the primitive mantle as calculated assuming the basaltic achondrite best initial (BABI) $^{87}Sr/^{86}Sr$ of 0.69897 (Papanastassiou and Wasserburg, 1968) and a primitive-mantle Rb/Sr of 0.2940 (Hofmann, 1988). TTGs formed before c. 3.45 Ga show a steady decrease in $^{87}Sr/^{86}Sr_i$ with time from values that have more radiogenic $^{87}Sr/^{86}Sr$ than a hypothetical Archean primitive mantle (AGC, BC; 3.62–3.50 Ga) to values that match those of such mantle (BGGT; c. 3.44 Ga). The weighted mean $^{87}Sr/^{86}Sr_i$ value of 0.7027 ± 0.0006, as obtained for multiple apatite inclusions in 3.72-Ga zircon grains from the Acasta Gneiss (Emo et al., 2018), is on this same trend. Given these consistencies and the different degree of ^{87}Sr enrichment during secondary processes, this trend seems geologically meaningful and indicates that the $^{87}Sr/^{86}Sr_i$ values of TTG sources underwent a steady decline during the Eo- and Paleoarchean. Although absent before 3.5 Ga, low $^{87}Sr/^{86}Sr_i$ values similar to those observed for the youngest BGGT TTG intrusions are common among younger TTGs; $^{87}Sr/^{86}Sr_i$ values observed among the 2.73–2.71 Ga

SAGB TTGs are equally unradiogenic. Similar $^{87}Sr/^{86}Sr_i$ values were observed for 3.30–3.25 Ga TTGs from the Dharwar Craton (Ravindran et al., 2020). The isotope data together provide evidence that there may have been systematic global changes in the Sr isotope composition of the sources of TTG magmas during the Archean. These changes likely relate to, and thus could inform on, changes in the average age of the source of these magmas. The latter can be investigated when considering the process of TTG petrogenesis.

TTGs and related granitoid magmas are generally considered to have formed via a two-stage process involving partial melting of a mantle source to form basalts, and the subsequent melting of this basalt as mafic source after its transformation to eclogite or amphibolite (e.g., Hoffmann et al., 2011; Rapp and Watson, 1995). This model is consistent with Hf isotope data from TTGs from the Bastar Craton, which indicate formation from variably aged mafic precursors (Maltese et al., 2021). Like these Hf isotope compositions, the lowest $^{87}Sr/^{86}Sr_i$ values of TTGs capture an isotope composition that is evolved from the $^{87}Sr/^{86}Sr$ composition of the source at the time of melt extraction. Divergence from primitive or depleted mantle trends may be more pronounced and resolvable for Sr, owing to stronger parent/daughter element fractionation between mafic and ultramafic rocks, and a relatively short half-life of ^{87}Rb compared to ^{147}Sm and ^{176}Lu. Assuming relative compositional uniformity among these sources, the $^{87}Sr/^{86}Sr_i$ of a TTG thus may provide a measure of the age or crustal residence time of the mafic TTG sources at the time of melting. The $^{87}Sr/^{86}Sr_i$ of a TTG ($^{87}Sr/^{86}Sr_{i,TTG}$) thus can be defined as a function of the $^{87}Sr/^{86}Sr_i$ of the amphibolite/eclogite source (AS) at the time of its extraction from its mantle source ($^{87}Sr/^{86}Sr_{i,AS}$), the average age of the AS, since extraction, at the time of TTG magmatism (t_{AS}), and the average Rb/Sr value of the AS ($^{87}Rb/^{86}Sr_{AS}$). The age t_{AS} can be resolved from this relationship through the modified decay eq. 1:

$$t_{AS} = \left(\lambda^{87}Rb\right)^{-1} Ln \left[\left[\left(^{87}Sr/^{86}Sr\right)_{i,TTG} - \left(^{87}Sr/^{86}Sr\right)_{i,AS} \right] \left(^{87}Rb/^{86}Sr\right)_{AS}^{-1} + 1 \right] \quad (1)$$

The values of $^{87}Sr/^{86}Sr_{i,AS}$ correspond to that of the reservoir that the AS was extracted from, presumably a depleted upper mantle (e.g., Maltese et al., 2021). The age since which significant mantle depletion has been initiated is not exactly known (4.44–4.08 Ga or even later; Amelin et al., 2000; Fisher and Vervoort, 2018; Petersson et al., 2019). It is possible that episodic depletion and crustal recycling during the Archean caused non-linear Sr-isotope evolution, as it appears to be recorded in the evolution of initial Nd and Hf isotope compositions (Bennett et al., 1993; Vervoort and Blinchert-Toft, 1999). When estimating t_{AS}, however, the relatively large uncertainties on $^{87}Sr/^{86}Sr_{i,TTG}$ result in large uncertainties of the time estimates for mantle extraction of AS. For simplicity, $^{87}Sr/^{86}Sr_{i,AS}$ is set equal to the $^{87}Sr/^{86}Sr$ of a generic average depleted mantle (DM) at the time of AS extraction and is estimated using a DM $^{87}Rb/^{86}Sr$ value of 0.0260 (Salters and Stracke, 2004) and assuming incompatible-element depletion of the mantle since 4.0 Ga (Amelin et al., 2000; Hawkesworth et al., 2010). The value of $^{87}Rb/^{86}Sr_{AS}$ is based on the composition of average Archean amphibolite (46 ppm Rb, 258 ppm Sr; Gao et al., 1998), which is consistent with the enriched nature of source amphibolites relative to modern MORB (Martin et al., 2014). The t_{AS} estimate obtained through this approach for 3.72 Ga Acasta Gneiss is 0.45–0.55 Ga, which implies AS extraction at c. 4.2 Ga. This is equal to the age of the oldest zircon from these rocks (Iizuka et al., 2006) and is generally considered a plausible age of the source of the Acasta Gneiss, i.e., on the basis of Hf isotopes in zircon and whole rock $^{147,146}Sm$-$^{143,142}Nd$ systematics (Bauer et al., 2017; Roth et al., 2014).

5.3. The changing age of TTG sources during Archean

Contributions from distinctly older (Eoarchean) crustal material to newly formed TTG crust have been widely recognized in the Hf isotope compositions of TTGs formed between 3.70 and 3.45 Ga (e.g., Bauer et al., 2017; Maltese et al., 2021; Næraa et al., 2012; Vervoort and Blinchert-Toft, 1999); Hf and Nd isotope composition that are more juvenile than indicated by the Sr isotope values for TTGs of a given age and terrane are observed for several cases, e.g., in the AGC and BGGT (e. g., Hoffmann et al., 2016), the BC (Maltese et al., 2021), SC (Pandey et al., 2019; Upadhyay et al., 2014). This apparent discrepancy could indicate that even the least radiogenic Sr isotope compositions of these rocks may not be entirely pristine. However, it could also reflect the more pronounced Rb/Sr fractionation during crust-mantle differentiation and stronger sensitivity of the Rb-Sr system to crustal residence time. Accounting for the geological history of the TTG precursor rocks it thus important for the adequate interpretation of radiogenic isotope ratios of TTGs. Although the Sr isotope record is still very limited for this time period, the data obtained so far are consistent with aged mafic sources. These granitoid rocks appear to have been derived from mafic sources that were extracted from the mantle an average c. 0.5 Gyr before producing TTG magmas. The Hf isotope compositions of these rocks become increasingly less radiogenic with time (Bauer et al., 2017; Hoffmann et al., 2011). Consistent with this, the $^{87}Sr/^{86}Sr_i$ of various TTGs produced after 3.45 Ga (e.g., SAGB, Dharwar) are distinctly different from Eoarchean TTGs in that their $^{87}Sr/^{86}Sr_i$ are less radiogenic and their source rocks appear to have generally been no older than 0.2 Gyr. The Greenlandic TTGs from the KB and TT may be considered an exception, as their $^{87}Sr/^{86}Sr_i$ are relatively radiogenic (0.7024–0.7026; Fig. 5). These values could reflect assimilation of Eoarchean cratonic crust of this region (Nutman et al., 1996; Amelin et al., 2010; Fisher and Vervoort, 2018); the TT is directly juxtaposed to the Mesoarchean Akia Terrane, which appears to have an Eoarchean mafic source (Gardiner et al., 2019) and comprises lithologies that are largely similar in age and rock assemblage to those of the TT. Alternatively, the $^{87}Sr/^{86}Sr_i$ values obtained from the TT and KB samples may overestimate actual $^{87}Sr/^{86}Sr_i$. The analyzed apatite grains from the KB are relatively large and thus possibly represent matrix grains that, like matrix grains in other samples, underwent secondary ^{87}Sr enrichment. Inclusions of apatite in other minerals were analyzed for a 2.85 Ga sample from the TT, but these inclusions are few and $^{87}Sr/^{86}Sr_i$ estimates are not fully consistent. The $^{87}Sr/^{86}Sr_i$ estimated for the WKS-E sanukitoids is similar to that of TTGs of the same age. Unlike TTGs, sanukitoids form by the flux melting subcontinental lithospheric mantle that is metasomatized or enriched with recycled continental crust (Heilimo et al., 2011; Laurent et al., 2014; Smithies et al., 2019). The $^{87}Sr/^{86}Sr_i$ values of the analyzed sanukitoid samples are undistinguishable from depleted-mantle values. Considering that recycled continental crust dominates the Sr budget of any mantle source that it contaminated, it is unlikely that such crust was present in the source of these rocks. The cause for the incompatible-element enrichment of sanukitoids thus must be sought in the slab- or mantle-derived fluids that metasomatized the source of such rocks.

A similar kind of transition towards, on average, more depleted mantle-like isotope compositions has been observed in the Hf isotope records of zircon from many Archean TTG occurrences worldwide (Bauer et al., 2017; Bauer et al., 2020; Hoffmann and Kröner, 2019; Kröner et al., 2014; Mulder et al., 2021; Næraa et al., 2012). The age of this transition appears to be different among Archean terranes. Hafnium isotope data from Greenlandic TTGs indicate that such transition occurred at 3.3–3.2 Ga, when particularly radiogenic compositions became prevalent (Kirkland et al., 2021). Still, the paucity of Hf isotope data for 3.5–3.3 Ga TTGs from this area and the observation of radiogenic Hf compositions in TTGs of such age in other Archean cratons (Roberts and Spencer, 2014) leave the possibility that this transition occurred earlier there, as it appears to have done in the Yilgarn, Kaapvaal and Slave cratons (e.g., Bauer et al., 2020; Hoffmann and Kröner, 2019; Mulder et al., 2021). The new Sr isotope data indicates that the transition towards particularly juvenile TTG sources occurred in a relatively short time period of <0.2 Gyr (3.60–3.45 Ga) and is recorded

seemingly synchronously in cratonic fragments of different paleogeographic location and descent. This indicates that the transition was a global phenomenon thus had a possible global cause.

Two possible causes may explain the rising predominance juvenile TTG sources at c. 3.5 Ga: (1) the definitive recycling into the mantle of a long-lived mafic reservoirs that served as sources for Eoarchean TTGs (e. g., Hadean high-U/Pb mafic crust; Kamber, 2015, 2) the onset of an additional, much more efficient crustal growth mechanism that involved melting of mafic source rocks more shortly after their mantle extraction than was possible until then. Although these causes need not be related, they would both be logical consequences of geodynamic change – specifically enhanced global plate motion and the onset of mobile lid tectonics. Mobile lid tectonics would involve zones of downwelling or subduction, which would enable more efficient recycling of ancient lithosphere, while providing a new mechanism for the melting of young mafic crust in the form of oceanic plates. The trends in Sr isotopes, like those seen in Hf isotopes (Bauer et al., 2020; Næraa et al., 2012), thus could trace secular geodynamic change following the Eoarchean. Alternatively, more widespread mantle melting due to increased mantle potential temperatures would provide a mechanism that would dilute ancient crustal reservoirs, while replenishing the crust with voluminous juvenile crust (Kirkland et al., 2021). This would provide an explanation for the same temporal evolution in radiogenic isotope signatures without requiring a fundamental shift in global geodynamics. Regardless of which process was responsible, the Sr isotopes provide independent evidence for a systematic, global change in the average age of TTG sources at c. 3.5 Ga and confirm the interpretation from Hf isotopes (Belousova et al., 2010; Roberts and Spencer, 2014) that juvenile sources were the norm for TTGs produced since then. This change was seemingly irreversible and marked the definitive loss of the ancient long-lived mafic reservoirs that served as main TTG sources during and before the Eoarchean.

6. Conclusions

- In-situ Sr isotope analysis of apatite by LA-MC-ICPMS constrain the initial $^{87}Sr/^{86}Sr$ ($^{87}Sr/^{86}Sr_i$) values of Archean TTGs and related rocks, including sanukitoids, throughout the Archean. The record obtained in this study covers TTGs of different Archean age (3.62–2.68 Ga) from cratons of different geographical locations.
- Apatite inclusions in primary magmatic minerals typically yielded lowest $^{87}Sr/^{86}Sr$ values in a given sample, indicating partial shielding from re-equilibration by host phases. Elevated $^{87}Sr/^{86}Sr$ values in some inclusions and in apatite in other textural settings (embedded in magmatic minerals, or located in matrices) indicate local re-equilibration with, and enrichment of ^{87}Sr from, K-rich phases in the rocks, adding merit to the general interpretation that lowest $^{87}Sr/^{86}Sr$ values best approximate $^{87}Sr/^{86}Sr_i$.
- $^{87}Sr/^{86}Sr_i$ estimates obtained from apatite provide firm time-resolved constraints on the changing age of the sources of Archean granitoids. TTGs emplaced before 3.45 Ga exhibit radiogenic $^{87}Sr/^{86}Sr_i$ values, indicating derivation from old (0.2–0.5 Gyr) mafic sources. The $^{87}Sr/^{86}Sr_i$ values of younger TTGs and Neoarchean sanukitoids are generally less radiogenic, tracing closely the Sr isotope evolution of the depleted mantle.
- The Sr isotope record, widely sampled in this study, indicates that the change from old to young TTG sources was a global phenomenon that occurred within a relatively short time window (3.60–3.45 Ga). This time interval marks a distinct and irreversible change in the processes and efficiency of continental crust formation.

Supplementary data to this article can be found online at https://doi.org/10.1016/j.lithos.2022.106830.

Declaration of Competing Interest

The authors declare to not have any competing interests.

Acknowledgements

References

Agangi, A., Hofmann, A., Elburg, M.A., 2018. A review of Palaeoarchaean felsic volcanism in the eastern Kaapvaal craton: linking plutonic and volcanic records. Geoscience Frontiers 9, 667–688.

Amelin, Y., Lee, D.C., Halliday, A.N., Pidgeon, R.T., 1999. Nature of the Earth's earliest crust from hafnium isotopes in single detrital zircons. Nature 399, 252–255.

Amelin, Y., Kamo, S.L., Lee, D.-C., 2010. Evolution of early crust in chondritic or non-chondritic Earth inferred from U–Pb and Lu–Hf data for chemically abraded zircon from the Itsaq Gneiss Complex, West Greenland. Canadian Journal of Earth Sciences 48, 141–160.

Amelin, Y., Lee, D.C., Halliday, A.N., 2000. Early-middle archaean crustal evolutioin deduced from Lu-Hf and U-Pb isotopic studies of single zircon grains. Geochimica et Cosmochimica Acta 64, 4205–4225.

Anhaeusser, C.R., 2010. Magmatic and structural characteristics of the ca. 3440 Ma Theespruit pluton, Barberton mountain land, South Africa. American Journal of Science 310, 1136–1167.

Armstrong, R.A., 1968. A model for the evolution of strontium and lead isotopes in a dynamic Earth. Reviews of Geophysics 6, 175–199.

Arndt, N.T., 2013. The formation and evolution of the continental crust. Geochemical Perspectives Letters 2, 405–533.

Ayer, J., Amelin, Y., Corfu, F., Kamo, S., Ketchum, J., Kwok, K., Trowell, N., 2002. Evolution of the southern Abitibi greenstone belt based on U-Pb geochronology: autochthonous volcanic construction followed by plutonism, regional deformation and sedimentation. Precambrian Research 115, 63–95.

Bauer, A.M., Fisher, C.M., Vervoort, J.D., Bowring, S.A., 2017. Coupled zircon Lu-Hf and U-Pb isotopic analyses of the oldest terrestrial crust, the <4.03 Ga Acasta Gneiss Complex. Earth and Planetary Science Letters 458, 37–48.

Bauer, A.M., Reimink, J.R., Chacko, T., Foley, B.J., Shirey, S.B., Pearson, D.G., 2020. Hafnium isotopes in zircons document the gradual onset of mobile-lid tectonics. Geochemical Perspectives Letters 14, 1–6.

Bédard, J.H., 2020. From the LIPS of a serial killer: endogenic retardation of biological evolution on unstable stagnant-lid planets. Planetary and Space Science 192, 1–10.

Belousova, E.A., Kostitsyn, Y.A., Griffin, W.L., Begg, G.C., O'Reilly, S.Y., Pearson, N.J., 2010. The growth of the continental crust: constraints from zircon Hf-isotope data. Lithos 119, 457–466.

Bennett, V.C., Nutman, A.P., McCulloch, M.T., 1993. Nd isotopic evidence for transient, highly depleted mantle reservoirs in the early history of the Earth. Earth and Planetary Science Letters 119, 299–317.

Bizzarro, M., Simonetti, A., Stevenson, R.K., Kurszlaukis, S., 2003. In situ $^{87}Sr/^{86}Sr$ investigation of igneous apatites and carbonates using laser ablation MC-ICP-MS. Geochimica et Cosmochimica Acta 67, 289–302.

Bleeker, W., 2003. The late Archean record: a puzzle in ca. 35 pieces. Lithos 71, 99–134.

Corfu, F., 1993. The evolution of the southern Abitibi greenstone belt in light of precise U-Pb geochronology. Economic Geology 88, 1323–1340.

Debaille, V., O'Neill, C., Brandon, A.D., Haenecour, P., Yin, Q.-Z., Mattielli, N., Treiman, A.H., 2013. Stagnant-lid tectonics in early Earth revealed by ^{142}Nd variations in late Archean rocks. Earth and Planetary Science Letters 373, 83–92.

Dhuime, B., Hawkesworth, C.J., Cawood, P.A., Storey, C.D., 2012. A change in the geodynamics of continental growth 3 billion years ago. Science 335, 1334–1336.

Emo, R.B., Smit, M.A., Schmitt, M., Kooijman, E., Scherer, E.E., Sprung, P., Bleeker, W., Mezger, K., 2018. Evidence for evolved Hadean crust from Sr isotopes in apatite within Eoarchean zircon from the Acasta Gneiss complex. Geochimica et Cosmochimica Acta 235, 450–462.

Fisher, C.M., Vervoort, J.D., 2018. Using the magmatic record to constrain the growth of continental crust—the Eoarchean zircon Hf record of Greenland. Earth and Planetary Science Letters 488, 79–91.

Foley, S., Tiepolo, M., Vannucci, R., 2002. Growth of early continental crust controlled by melting of amphibolite in subduction zones. Nature 417, 837–840.

Friend, C.R.L., Nutman, A.P., 2001. U–Pb zircon study of tectonically bounded blocks of 2940–2840 Ma crust with different metamorphic histories, Paamiut region, South-West Greenland: implications for the tectonic assembly of the North Atlantic craton. Precambrian Research 105, 143–164.

Gao, S., Luo, T.-C., Zhang, B.-R., Zhang, H.-F., Han, T.-W., Zhao, Z.-D., Hu, Y.-K., 1998. Chemical composition of the continental crust as revealed by studies in East China. Geochimica et Cosmochimica Acta 62, 1959–1975.

Gardiner, N.J., Kirkland, C.L., Hollis, J., Szilas, K., Steenfelt, A., Yakymchuk, C., Heide-Jørgensen, H., 2019. Building Mesoarchean crust upon Eoarchean roots: the Akia Terrane, West Greenland. Contributions to Mineralogy and Petrology 174, 1–19.

Gerya, T.V., 2014. Precambrian geodynamics: concepts and models. Gondwana Research 25, 442–463.

Ghosh, J.G., 2004. 3.56 Ga tonalite in the central part of the Bastar Craton, India: oldest Indian date. Journal of Asian Earth Sciences 23, 359–364.

Gillespie, J., Nemchin, A.A., Kinny, P.D., Martin, L., Aleshin, M., Roberts, M.P., Ireland, T.R., Whitehouse, M.J., Jeon, H., Cavosie, A.J., Kirkland, C.L., 2021. Strontium isotope analysis of apatite via SIMS. Chemical Geology 559, 1–8.

Glodny, J., Grauert, B., 2009. Evolution of a hydrothermal fluid-rock interaction system as recorded by Sr isotopes: a case study from the Schwarzwald, SW Germany. Mineralogy and Petrology 95, 163–178.

Halla, J., 2002. Origin and Paleoproterozoic Reactivation of Neoarchean High-K Granitoid Rocks in Eastern Finland. Annales Academiae Scientiarum Fennicae, Geologica-Geographica, p. 163.

Halla, J., 2005. Late Archean high-Mg granitoids (sanukitoids) in the southern Karelian domain, eastern Finland: Pb and Nd isotopic constraints on crust—mantle interactions. Lithos 79, 161–178.

Hawkesworth, C.J., Dhuime, B., Pietranik, A.B., Cawood, P.A., Kemp, A.I.S., Storey, C.D., 2010. The generation and evolution of the continental crust. Journal of the Geological Society of London 167, 229–248.

Heilimo, E., Halla, J., Huhma, H., 2011. Single-grain zircon U-Pb age constraints of the western and eastern sanukitoid zones in the Finnish part of the Karelian Province. Lithos 121, 87–99.

Hoffmann, J.E., Kröner, A., 2019. Early Archean crustal evolution in southern Africa—an updated record of the Ancient Gneiss Complex of Swaziland. In: van Kranendonk, M.J., Bennett, V.C., Hoffmann, J.E. (Eds.), Earth's Oldest Rocks, 2nd edition. Elsevier, Amsterdam, pp. 553–567.

Hoffmann, J.E., Münker, C., Næraa, T., Rosing, M.T., Herwartz, D., Garbe-Schönberg, D., Svahnberg, H., 2011. Mechanisms of archean crust formation inferred from high-precision HFSE systematics in TTGs. Geochimica et Cosmochimica Acta 75, 4157–4178.

Hoffmann, J.E., Kröner, A., Hegner, E., Viehmann, S., Xie, H., Iaccheri, L.M., Schneider, K.P., Hofmann, A., Wong, J., Geng, H., Yang, J., 2016. Source composition, fractional crystallization and magma mixing processes in the 3.48-3.43 Tsawela tonalite suite (Ancient Gneiss Complex, Swaziland). – Implications for Palaeoarchaean geodynamics. Precambrian Research 276, 43–66.

Hofmann, A.W., 1988. Chemical differentiation of the Earth: the relationship between mantle, continental crust, and oceanic crust. Earth and Planetary Science Letters 90, 297–314.

Hölttä, P., Heilimo, E., Huhma, H., Juopperi, H., Kontinen, A., Konnunaho, J., Lauri, L., Mikkola, P., Paavola, J., Sorjonen-Ward, P., 2012. Archean complexes of the Karelia province in Finland. Geological Survey of Finland Special Paper 54, 9–20.

Hurley, P.M., Hughes, H., Faure, G., Fairbairn, H.W., Pinson, W.H., 1962. Radiogenic strontium-87 model of continent formation. Journal of Geophysical Research 67, 5315–5334. https://doi.org/10.1029/jz067i013p05315.

Iizuka, T., Horie, K., Komiya, T., Maruyama, S., Hirata, T., Hidaka, H., Windley, B.F., 2006. 4.2 Ga zircon xenocryst in an Acasta gneiss from northwestern Canada: evidence for early continental crust. Geology 34, 245–248.

Jenkin, G.R.T., Ellam, R.M., Rogers, G., Stuart, F.M., 2001. An investigation of closure temperature of the biotite Rb-Sr system: the importance of cation exchange. Geochimica et Cosmochimica Acta 65, 1141–1160.

Johnson, T.E., Brown, M., Gardiner, N.J., Kirkland, C.L., Smithies, R.H., 2017. Earth's first stable continents did not form by subduction. Nature 543, 239–242.

Kamber, B.S., 2015. The evolving nature of terrestrial crust from the Hadean, through the Archaean, into the Proterozoic. Precambrian Research 258, 48–82.

Kamo, S.L., Davis, D.W., 1994. Reassessment of Archean crustal development in the Barberton Mountain Land, South Africa, based on U-Pb dating. Tectonics 13, 167–192.

Kirkland, C.L., Hartnady, M.I.H., Barham, M., Olierook, H.K.H., Steenfelt, A., Hollis, J.A., 2021. Widespread reworking of Hadean-to-Eoarchean continents during Earth's thermal peak. Nature Communications 12, 1–9.

Kolb, J., Kokfelt, T.F., Dziggel, A., 2012. Geodynamic setting and deformation history of an Archaean terrane at mid- crustal level: the Tasiusarsuaq terrane of southern West Greenland. Precambrian Research 212-213, 34–56.

Kröner, A., Hoffmann, J.E., 2016. Post-Badplaas workshop excursion. In: Kröner, A. (Ed.), Badplaas Field Workshop on Archaean Geodynamics, Excursion Guidebook. 35th International Geological Congress Foundation, Johannesburg, South Africa (54 pp.).

Kröner, A., Hoffmann, J.E., Xie, H., Münker, C., Hegner, E., Wan, Y., Hofmann, A., Liu, D., Yang, J., 2014. Generation of early Archaean grey gneisses through melting of older crust in the eastern Kaapvaal craton, southern Africa. Precambrian Research 255, 823–846.

Laurent, O., Martin, H., Moyen, J.F., Doucelance, R., 2014. The diversity and evolution of late-Archean granitoids: evidence for the onset of "modern-style" plate tectonics between 3.0 and 2.5 Ga. Lithos 205, 208–232.

London, D., Wolf, M.B., Morgan, G.B.V.I., Garrido, M.G., 1999. Experimental silicate–phosphate equilibria in peraluminous granitic magmas, with a case study of the Alburquerque batholith at Tres Arroyos, Badajoz, Spain. Journal of Petrology 40, 215–240.

Maltese, A., Mezger, K., Upadhyay, D., Berndt, J., Scherer, E.E., 2021. On the petrogenesis of Paleoarchean continental crust: U-Pb-Hf and major trace-element constraints from the Bastar Craton, India. Chemical Geology 579, 1–14.

Martin, H., Smithies, R.H., Rapp, R., Moyen, J.F., Champion, D., 2005. An overview of adakite, tonalite- trondhjemite-granodiorite (TTG), and sanukitoid: relationships and some implications for crustal evolution. Lithos 79, 1–24.

Martin, H., Moyen, J.-F., Guitreau, M., Blichert-Toft, J., Le Pennec, J.-L., 2014. Why Archean TTG cannot be generated by MORB melting in subduction zones. Lithos 198-199, 1–13.

McDonough, W.F., Sun, S.-S., 1995. The composition of the Earth. Chemical Geology 120, 223–253.

Moorbath, S., Pankhurst, R.J., 1976. Further rubidium-strontium age and isotope evidence for the nature of the late Archaean plutonic event in West Greenland. Nature 262, 124–126.

Moore, L.J., Murphy, T.J., Barnes, I.L., Paulsen, P.J., 1982. Absolute isotopic abundance ratios and atomic weight of a reference sample of strontium. Journal of Research of the National Bureau of Standards 87, 1–8.

Moyen, J.F., Martin, H., 2012. Forty years of TTG research. Lithos 148, 312–336.

Moyen, J.F., Stevens, G., Kisters, A.F.M., Belcher, R.W., 2007. TTG plutons of the Barberton granitoid- greenstone terrain, South Africa. In: van Kranendonk, M.J., Smithies, R.H., Bennett, V.C. (Eds.), Earth's Oldest Rocks. Elsevier, Amsterdam, pp. 607–667.

Mulder, J.A., Nebel, O., Gardiner, N.J., Cawood, P.A., Wainwright, A.N., Ivanic, T.J., 2021. Crustal rejuvenation stabilized Earth's first cratons. Nature Communications 12, 1–7.

Mutanen, T., Huhma, H., 2003. The 3.5 Ga Siurua trondhjemite gneiss in the Archean Pudasjärvi Granulite Belt, northern Finland. Bulletin of the Geological Society of Finland 75, 51–68.

Næraa, T., Scherstén, A., Rosing, M.T., Kemp, A.I.S., Hoffmann, J.E., Kokfelt, T.F., Whitehouse, M.J., 2012. Hafnium isotope evidence for a transition in the dynamics of continental growth 3.2 Gyr ago. Nature 485, 627–630.

Nagel, T.J., Hoffmann, J.E., Münker, C., 2012. Generation of Eoarchean tonalite-trondhjemite-granodiorite series from thickened mafic crust. Geology 40, 375–378.

Nebel, O., Scherer, E.E., Mezger, K., 2011. Evaluation of the [87]Rb decay constant by age comparison against the U-Pb system. Earth and Planetary Science Letters 301, 1–8.

Nutman, A.P., McGregor, V.R., Friend, C.R.L., Bennett, V.C., Kinny, P.D., 1996. The Itsaq Gneiss Complex of southern West Greenland; the world's most extensive record of early crustal evolution (3900-3600 Ma). Precambrian Research 78, 1–39.

Palin, R.M., White, R.W., Green, E.C.R., 2016. Partial melting of metabasic rocks and the generation of tonalitic–trondhjemitic–granodioritic (TTG) crust in the Archean: Constraints from phase equilibrium modelling. Precambrian Research 287, 73–90.

Pandey, O.P., Mezger, K., Ranjan, S., Upadhyay, D., Villa, I.M., Nagler, T.F., Vollstaedt, H., 2019. Genesis of the Singhbhum Craton, eastern India: implications for Archean crust-mantle evolution of the Earth. Chemical Geology 512, 85–106.

Papanastassiou, D.A., Wasserburg, G.J., 1968. Initial strontium isotopic abundances and the resolution of small time differences in the formation of planetary objects. Earth and Planetary Science Letters 5, 361–376.

Petersson, A., Kemp, A.I.S., Hickman, A.H., Whitehouse, M.J., Martin, L., Gray, C.M., 2019. A new 3.59 Ga magmatic suite and a chondritic source to the east Pilbara Craton. Chemical Geology 511, 51–70.

Piccoli, P., Candela, P.A., 2002. Apatite in igneous systems. In: Kohn, M.J., Rakovan, J., Hughes, J.M. (Eds.), Phosphates – Reviews in Mineralogy and Geochemistry 48. Mineralogical Society of America, Washinton DC, pp. 255–292.

Rajesh, H.M., Mukhopadhyay, J., Beukes, N.J., Gutzmer, J., Belyanin, G.A., Armstrong, R.A., 2009. Evidence for an early Archaean granite from Bastar Craton, India. Journal of the Geological Society of London 166, 193–196.

Rapp, R.P., Watson, E.B., 1995. Dehydration of metabasalt at 8-32 kbar: implications for continental growth and crust-mantle recycling. Journal of Petrology 36, 891–931.

Rapp, R.P., Shimizu, N., Norman, M.D., 2003. Growth of early continental crust by partial melting of eclogite. Nature 425, 605–609.

Ravindran, A., Mezger, K., Balakrishnan, S., Kooijman, E., Schmitt, M., Berndt, J., 2020. Initial [87]Sr/[86]Sr as a sensitive tracer of Archaean crust-mantle evolution: constraints from igneous and sedimentary rocks in the western Dharwar Craton, India. Precambrian Research 337, 1–15.

Roberts, N.M.W., Spencer, C.J., 2014. The Zircon Archive of Continent Formation Through Time, 389. Geological Society, London, Special Publication, pp. 197–224.

Roth, A.S.G., Bourdon, B., Mojzsis, S.J., Rudge, J.F., Guitreau, M., Blichert-Toft, J., 2014. Combined [147,146]Sm-[143,142]Nd constraints on the longevity and residence time of early terrestrial crust. Geochemistry, Geophysics, Geosystems 15, 2329–2345.

Salters, V.J.M., Stracke, A., 2004. Composition of the depleted mantle. Geochemistry, Geophysics, Geosystems 5, 1–27.

Smit, M.A., Scherstén, A., Naeraa, T., Emo, R.B., Scherer, E.E., Sprung, P., Bleeker, W., Mezger, K., Maltese, A., Cai, Y., Rasbury, E.T., Whitehouse, M.J., 2019. Formation of Archean continental crust constrained by boron isotopes. Geochemical Perspectives Letters 12, 23–26.

Smithies, R.H., 2000. The Archaean tonalite-trondhjemite-granodiorite (TTG. series is not an analogue of Cenozoic adakite). Earth and Planetary Science Letters 182, 115–125.

Smithies, R.H., Lu, Y., Johnson, T.E., Kirkland, C.L., Cassidy, K.F., Champion, D.C., Mole, D.R., Zibra, I., Gessner, K., Sapkota, J., De Paoli, M.C., Poujol, M., 2019. No evidence for high-pressure melting of Earth's crust in the Archean. Nature Communications 10, 5559.

Tepper, J.H., Kuehner, S.M., 1999. Complex zoning in apatite from the Idaho batholith: A record of magma mixing and intracrystalline trace element diffusion. American Mineralogist 84, 581–595.

Upadhyay, D., Chattopadhyay, S., Kooijman, E., Mezger, K., Berndt, J., 2014. Magmatic and metamorphic history of Paleoarchean tonalite-trondhjemite-granodiorite (TTG. suite from the Singhbhum craton, eastern India). Precambrian Research 252, 180–190.

Vervoort, J.D., Blinchert-Toft, J., 1999. Evolution of the depleted mantle: Hf isotope evidence from juvenile rocks through time. Geochimica et Cosmochimica Acta 63, 533–556.

Wasserburg, G.J., Albee, A.L., Lanphere, M.A., 1964. Migration of radiogenic strontium during metamorphism. Journal of Geophysical Research 69, 4395–4401.

Watson, E.B., Harrison, T.M., Ryerson, F.J., 1985. Diffusion of Sm, Sr, and Pb in fluorapatite. Geochimica et Cosmochimica Acta 49, 1813–1823.

Windley, B.F., Garde, A.A., 2009. Arc-generated blocks with crustal sections in the North Atlantic craton of West Greenland: crustal growth in the Archean with modern analogues. Earth-Science Reviews 93, 1–30.

Yang, Y.H., Wu, F.Y., Yang, J.H., Chew, D.M., Xie, L.W., Chu, Z.Y., Zhang, Y.B., Huang, C., 2014. Sr and Nd isotopic compositions of apatite reference materials used in U–Th–Pb geochronology. Chemical Geology 385, 35–55.